

**Bristol, Glasgow, Imperial College London, University College London, Oxford,
Rutherford Appleton Laboratory**

in collaboration with

Aegean, Andrews, Argonne, Bologna, Bonn, Calabria, Chonnam, Columbia, DESY, DESY-Zeuthen, Florence, Freiburg, Hamburg, Jülich, Kazakhstan, KEK, Krakow, Kyungpook, Louvain, Madrid, McGill, Meiji Gakuin Univ., Moscow, NIKHEF, Ohio, Padova, Pennsylvania, Rome, Sagamihara, Santa Cruz, Seoul, Siegen, Tel Aviv, Tokyo, Tokyo Metropolitan Univ., Torino, Toronto, Warsaw, Weizmann Inst., Wisconsin, Yale, York (Ontario).

1 Introduction and Outlook

Much progress has been made in 2003 in overcoming the serious background problems encountered at HERA after the HERA II upgrade. As reported in the 2002 RAL Annual Report, the background levels made it impossible to take data at the anticipated luminosity and forced HERA to run at lower beam currents.

In January and February, ZEUS and H1 continued to take data to commission newly installed detectors and complete studies of the background problem. HERA was then shut down for nearly five months for the installation of extra shielding and the modification of collimators and other components. ZEUS took advantage of the shutdown to carry out work on several detectors. In particular, the CTD was modified to increase its efficiency at a lower HV setting.

HERA restarted in late July and began luminosity running again in October. It is now clear that the background situation has been vastly improved and no longer jeopardises the possibility of high luminosity running. The planned specific luminosity has been achieved, but there are limits at present on the machine currents. These are understood and work is in progress to overcome them. We therefore look forward to a rich programme of physics with high luminosity and polarised electron and positron beams.

In 2003 the UK teams continued to take responsibility for a wide range of activities within the ZEUS collaboration. The Physics Chairman is a UK physicist and the UK continued to provide the ZEUS tracking coordinator (until September), the Monte Carlo coordinator and the CTD coordinator. For at least part of the year, UK physicists have been joint coordinators for all four of the ZEUS physics groups.

Sections 2-5 of the report cover the status of the hardware that ZEUS UK is either responsible for or involved with, physics analysis topics are covered in Section 6 and factual information on theses, publications and talks is given in the appendices.

2 Central Tracking Detector

The Central Tracking Detector (CTD) is a large-volume, cylindrical drift chamber covering the central region ($15^\circ < \theta < 164^\circ$). It provides charged-particle tracking, momentum measurement and identification through dE/dx . It has been installed and operating successfully for 12 years. It also participates in all three levels of the ZEUS trigger.

The CTD's 4608 sense wires are arranged in nine superlayers, superlayer one being the innermost. The wires in odd-numbered superlayers run parallel to the chamber axis, whilst those in even-numbered layers have a small stereo angle ($\approx 5^\circ$). Taken together they provide

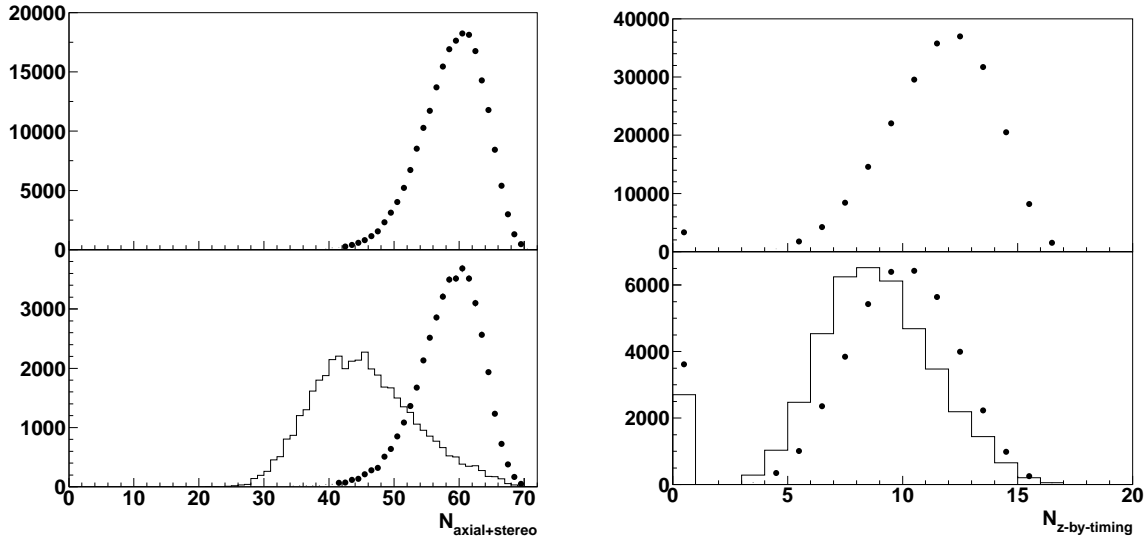


Figure 1: Number of FADC hits (left hand plots) and z-by-timing hits (right hand plots) matched to full length tracks reconstructed in the CTD. The top plots show the 2000 data, the solid histograms in the bottom plots show the 2002 data with 95% chamber HV and the other bottom plots are taken from the recent 2003 running period after the increase in postamplifier gains.

sufficient information to reconstruct tracks in three dimensions. All sense wires in the chamber are equipped with Flash Analogue-to-Digital Conversion (FADC) electronics and, in addition, all wires in superlayer one and the odd-numbered wires in superlayers three and five have z -by-timing electronics for the first-level trigger.

The CTD has continued to be one of the few components that can provide information on the nature of the backgrounds in the interaction region. Last year analysis of data from the CTD was central to the diagnosis of the background problems in the machine. Since September, with the restart of the machine, the CTD has shown that the background problems are to a large extent now solved. As more normal data taking conditions have now been reached, day-to-day operation of the CTD can now be performed by the regular shift crew. The chamber has functioned reliably throughout the year.

In order to operate the CTD at the higher beam currents expected from the machine, with acceptable sense wire currents in the CTD, it was decided last year to run the CTD at 95% of the standard HERA-I high voltage settings. Extensive studies were made to optimise the CTD performance and led to a decision to increase the gain of the postamplifier cards in the readout by a factor of 2, to counteract the effect of the reduction of chamber gain on the tracking performance. This required a major hardware change to each readout channel but was completed successfully within two weeks during the summer shutdown. The CTD was subsequently used for running cosmic ray tests and for evaluating the effect of the HERA improvements on the level of the positron-induced backgrounds.

The track-finding efficiencies and resolutions are now being re-evaluated. Initial findings indicate that the FADC system performance is equivalent to that from HERA-I, both in terms of hit efficiencies and resolutions and of offline tracking performance. However, the z system seems to show some degradation with respect to HERA I. The effect of this on the ZEUS First Level Trigger (FLT) is under study and the options for mitigating the effect are being investigated. One measure of the offline tracking performance is the number of hits matched to reconstructed tracks as shown in Fig. 1 for a sample of deep inelastic scattering (DIS) events. It can be seen that the number of FADC hits matched to the tracks has not decreased between 2000 and 2003. The number of z hits matched to the tracks is lower than in 2000, although there is an improvement

over the 2002 data.

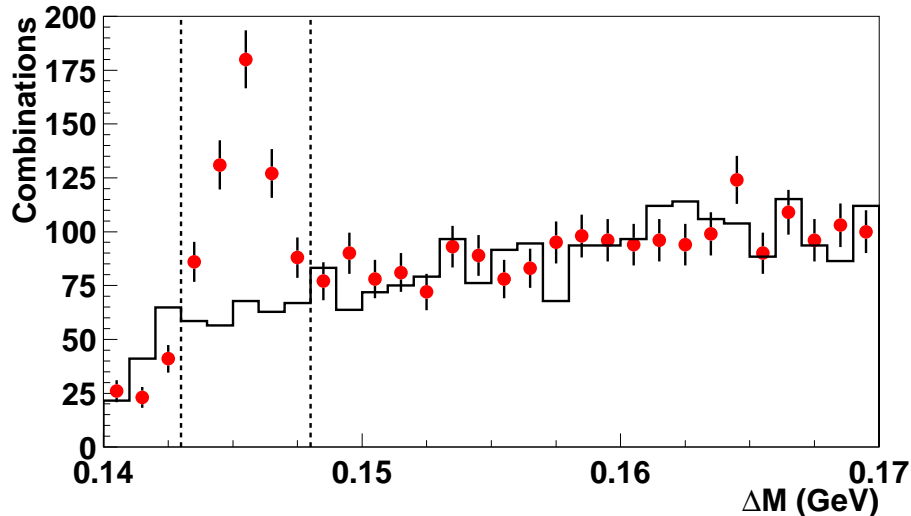


Figure 2: The mass difference distribution, $\Delta M = M(D^*) - M(D^0)$, during the recent luminosity running. The histogram shows the background distribution from wrong charge combinations.

In recent luminosity running, production of D^* mesons has been studied, as shown in Fig. 2. A clear signal is seen, with a width similar to that seen from HERA I data. Initial indications are that the production rate is approaching the expected level and that the offline tracking performance is sufficiently good for physics studies to be made.

Good use was made of the shutdown this year to ensure that sufficient spares are available. As there were not adequate spares for the FLT system, and given the importance of this for the experiment, dedicated effort was requested from RAL. This has yielded results in that there is now a functional test crate for the FLT hardware at RAL, and spares for the readout should be available soon. The infrastructure as a whole is in reasonable condition.

The continued operation and reliability of the CTD is of the utmost importance to the ZEUS experiment physics programme, and will remain so for the remainder of HERA running.

2.1 Triggering

ZEUS operates a three-level trigger, of which the first is a hardware-based system whose principal aim is to reduce backgrounds that do not come from the interaction point. CTD information is essential for this and the detector uses dedicated, pipelined processor cards which provide tracking information to the global first-level trigger. Because of the higher level of background the track triggers are of even greater importance than before. The first level track trigger continues to operate without modification, although with slightly lower efficiency than in 2000.

At the second level more precise software algorithms are used to clean the event sample further and classify certain types of physics events. Detailed tracking information is provided by the CTD second-level trigger which makes use of the data from all five axial superlayers and the z -by-timing information from layers 1, 3 and 5. It is at this level that the biggest changes to the trigger are being made, to take advantage of the extensions to ZEUS tracking (MVD and Forward Tracking) and the price-performance of PC hardware. Before the shutdown for the HERA upgrade, modifications were made to the CTD Transputer network in order to allow data from the FADC electronics to be sent to the new Global Tracking Trigger (GTT). The GTT hardware consists of Gigabit ethernet communications and a farm of 12 1GHz Linux PCs for processing. This augments the original CTD second level transputer based system and the farm

hardware has been funded through the Yale ZEUS group. The hardware is working and primary algorithms have been successfully evaluated, under recent luminosity data taking conditions. Modifications to the overall ZEUS trigger and DAQ system to make use of the algorithm results for online event selection are underway.

Studies of the adverse effect of reducing the CTD high voltage on the CTD SLT have been performed, and with modifications to the CTD readout, no significant loss of the vertex finding efficiency is observed, although there is a slight degradation of the vertex resolution.

2.2 CTD monitoring

The operation of the CTD is monitored by the ZEUS shift crew who check a small number of critical histograms. Members of the CTD Data Quality Monitoring (DQM) team, working from DESY or the UK, inspect further online plots as well as plots from the automatic analysis of data samples at 90-minute intervals. These samples are also used to calibrate the CTD. Finally, the DQM team checks the quality control plots from the initial reconstruction of all data to ensure that data is of adequate quality for physics analysis.

This procedure has been used for several years and has proved effective in the early diagnosis of problems. Some changes have been necessitated by the new running conditions after the HERA II upgrade and work continues to streamline the system for the smaller DQM team. However, the last few months have seen a resumption of routine data taking after a long break.

3 HERA Status and Backgrounds

The commissioning period for HERA and the experiments, begun in October 2002, continued for the first two months of 2003, aimed at diagnosing the background problems, whilst delivering luminosity to the experiment. UK members of ZEUS were closely involved with both the studies of the backgrounds and in recommissioning the detector with the first luminosity. Following this, there was a five months shutdown during which there were modifications close to the interaction point to reduce the level of backgrounds in the detector. Since October, despite several operational restrictions, there has been a period of stable running, which has provided physics quality luminosity for the detectors. The HERA delivered luminosity to date has been 6 pb^{-1} .

During 2002 it became clear that the backgrounds in the ZEUS detector were something like a factor 10 times larger than had been anticipated. A period of intense activity and close collaboration between the experimental groups and HERA machine physicists to pin down both the type and source of the backgrounds. There are at least three different components to the problem:

- off-momentum positrons in time with the positron beam;
- indirect synchrotron radiation back-scattered mainly from an absorber about 11 m on the upstream proton side of the ZEUS interaction point;
- a very large increase in proton beam-gas background, due to poor dynamic vacuum in the region immediately surrounding the interaction region. This was found to be the largest problem.

The CTD has been an essential tool in arriving at this understanding. It was expected that the backgrounds would inevitably be higher after the upgrade, particularly a higher level of synchrotron radiation caused by the more intensely focused beams and new optics needed for HERA-II. New interaction region collimators were designed to avoid any direct synchrotron radiation reaching the sensitive components of the detector. In this they have been successful,

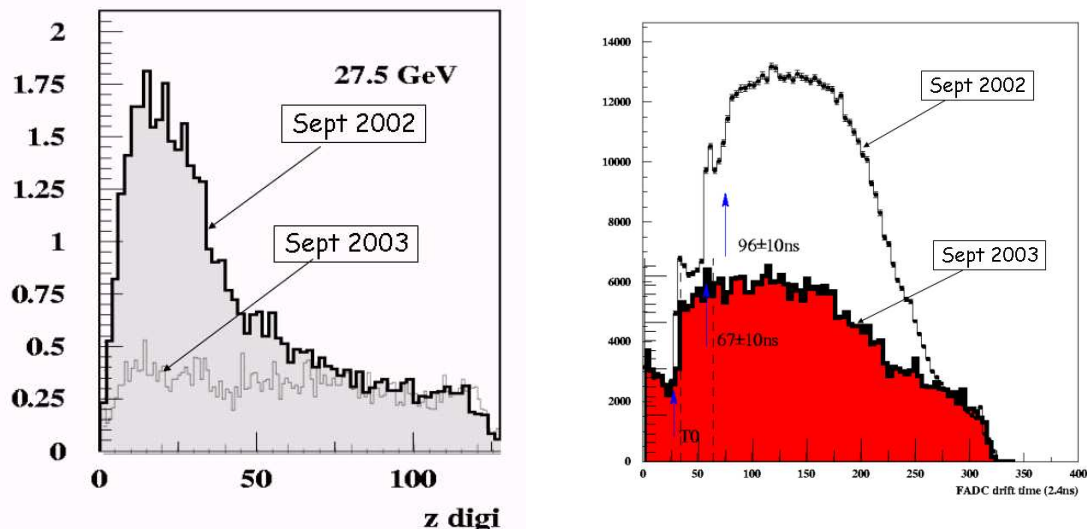


Figure 3: Distribution of CTD hits before and after the summer 2003 shutdown. The left hand plot shows the z distribution of CTD hits, the right hand plot the drift time distribution with respect to the HERA bunch crossing, marked TO on the plot. The major contributions from synchrotron radiation reflections are indicated.

unfortunately a rather large amount of radiation back-scattered mainly from the main absorber 11m from ZEUS was hitting the collimator nearest to the MVD and being scattered into the CTD. It was also expected that the vacuum in and around the interaction point would be worse because the new final-focus superconducting magnets, positioned just inside the ZEUS calorimeter on both sides, do not allow space for as many high-vacuum pumps as before. However whilst the static vacuum seemed not to be a problem, the dynamic vacuum (positron-beam induced degradation of the vacuum) was much worse than expected. The combination of a narrower beampipe, cold surfaces, more collimators, fewer pumps and new optics complicates the diagnosis of the problems.

To alleviate the problem of the reflected synchrotron radiation the collimator nearest the MVD was redesigned, and was installed in the shutdown this summer. The reduction in the reflected synchrotron radiation achieved is demonstrated in Fig.3, which shows the distributions of CTD hits before and after the summer 2003 shutdown. The z distribution of the hits is now flat, with the characteristic peak from the reflections having disappeared. The drift time distribution is now dominated by contributions in time with the beam, i.e. off-momentum positrons. The clear reflections seen in 2002 are no longer present. It can be concluded that the reflected synchrotron contribution to the background is now small.

The larger background problem was shown to be the proton-induced background, caused by the dynamic background effect, i.e. to a dramatic worsening of the vacuum near the interaction region proportional to the positron beam current. The measures taken to reduce the reflected synchrotron radiation are expected also to help reduce this dynamic background, as the subsequent heating of the beampipe would be reduced. In addition to try and reduce the higher-order mode heating of the beampipe during injection, better thermal conductivity between the collimators and the beampipe was introduced.

Changes in commissioning procedure were introduced to try and reduce the amount of gas “stored” in the beampipe walls: The beampipe near to the interaction region was heated prior to the luminosity running period, to try and free the gas present in the walls. In addition during August there was a period, where the machine ran with high positron currents for several weeks, to try and “bake-out” remnant gas from the beampipe walls. This combined with a

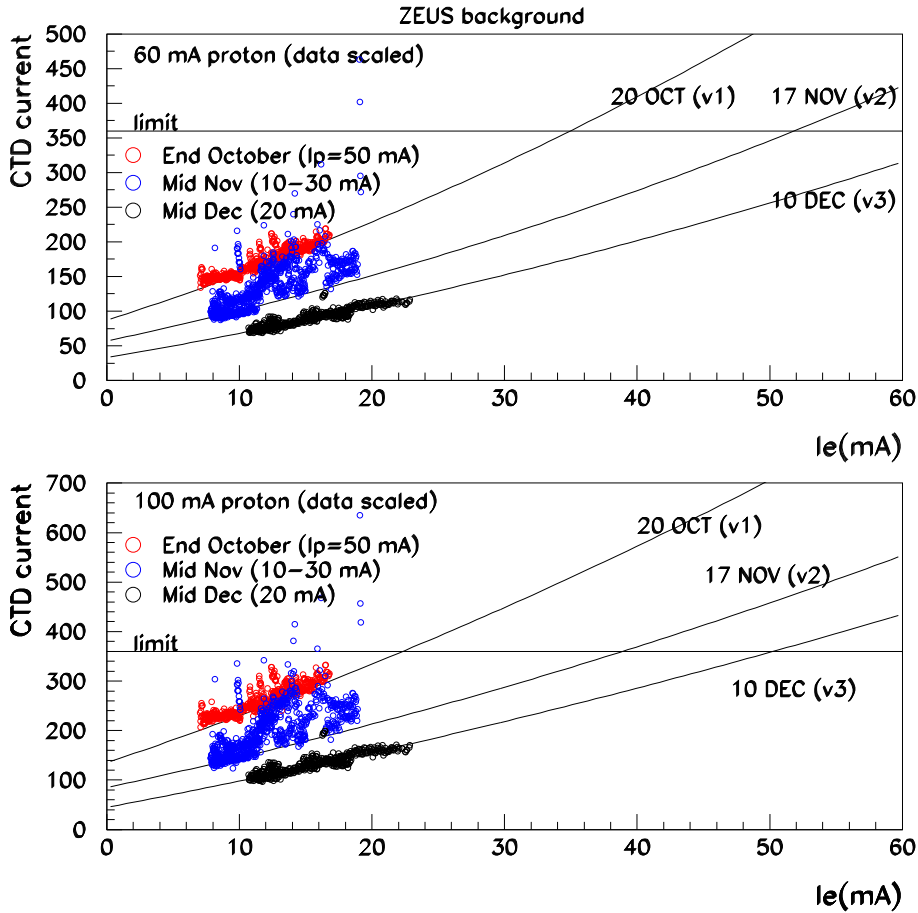


Figure 4: Recent background conditions in terms of the drawn CTD sense wire currents. The CTD currents drawn are rescaled to the proton currents indicated.

procedure for regular warm-ups of the cold final focusing magnets in the interaction regions to room temperature to remove frozen gas on the inner surface of the magnets was shown to significantly improve the observed dynamic vacuum.

The overall effect of these changes on the running conditions for the experiment can be demonstrated in Fig.4, which shows the measured CTD sense wire currents, normalised to particular proton beam currents. The improvement with time, at month intervals during the luminosity run, due to integrated positron beam current is clearly seen. It is positive to note that the improvements with time do not appear to have saturated yet. Extrapolating from the present running conditions, this shows that it should be possible to run the CTD within the safe operating limit on the sense wire currents even at the maximum predicted beam currents, indicating that the factor 8 improvement in the backgrounds may have been achieved.

4 Microvertex Detector (MVD)

MVD activities in 2003 were dominated by the long HERA shutdown required for the modifications to reduce the background problems. First, to allow access to the collimators inside the beampipe at the rear (electron beam) end of the MVD, required complete disconnection of all MVD-side cables at the patch-box, moving them away from the GG magnet and securing them safely. The GG magnet also had to be removed. After the changes to the collimators and insertion of some extra shielding (against synchrotron radiation) the whole procedure had to be reversed. As noted in the 2001 ZEUS Annual Report, getting the cables to fit around the

GG magnet in the space available, once the calorimeter was closed, was a very tricky task. The MVD-side cables and connectors are also quite delicate, so great care and effort had to be taken throughout these procedures. Both the uncabing and re-cabing were performed successfully by the Oxford crew of engineers and technicians who had done the job in the first place.

In parallel with this, and continuing through the period of HERA machine studies after the detector was closed, work was undertaken by the MVD group (not involving UK staff directly) to recover ‘bad modules’ and to improve aspects of the MVD data-acquisition procedures and the low-voltage control software. The MVD has a total of 412 silicon wafer plus readout ‘half-modules’ and by the time luminosity running resumed in October only 7 were not fully functional. During 2003 the track reconstruction and fitting software was also improved. The aim is to have complete integration of MVD, CTD and STT (straw tube forward tracker) tracking. As ever the forward direction is hardest with two new detectors and a complex magnetic field to contend with. MVD+CTD tracking is working well as is demonstrated by Fig. 5 showing a NC event with tracks reconstructed using hits in both detectors.

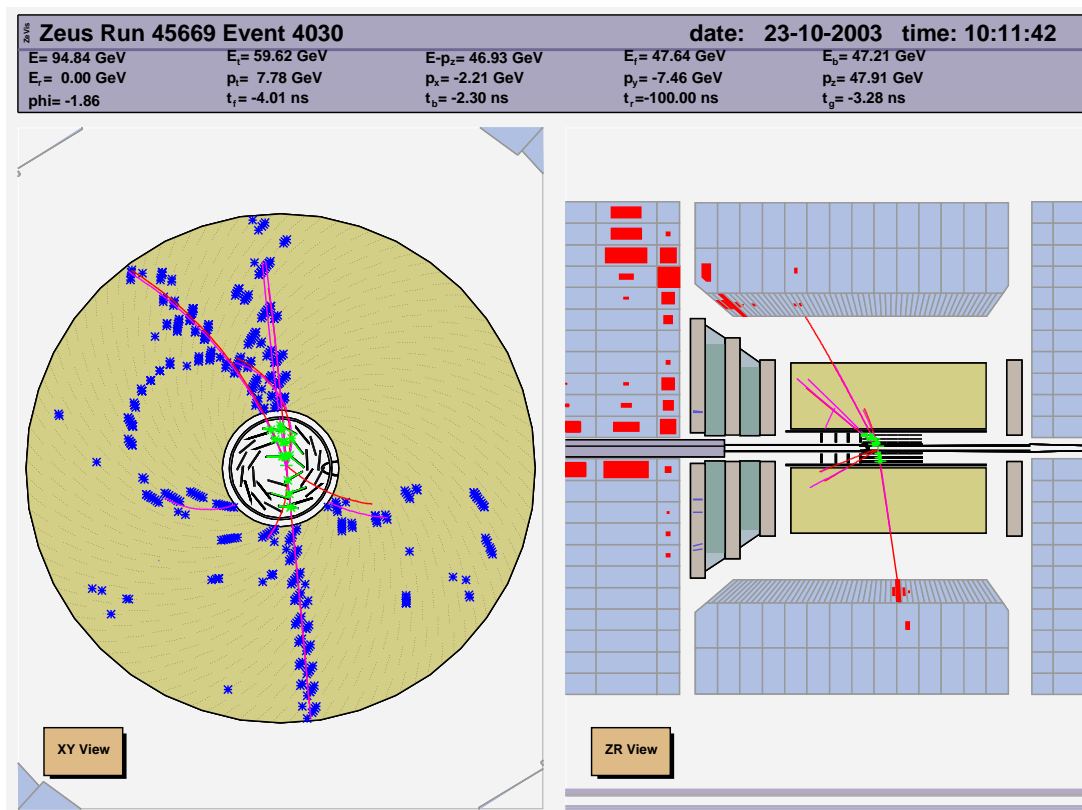


Figure 5: A high- Q^2 NC event recorded in ZEUS, showing charged particle tracks reconstructed using combined MVD+CTD hits.

Work continues on developing the procedures to analyse and use data from the MVD optical alignment system (provided and maintained by the UK). The system uses five infra-red laser beams passing through semi-transparent silicon strip detectors and relates the overall position of the MVD support tube to the CTD, as well as providing information on gross movements or distortion of the structure. Laser alignment runs are taken routinely as part of normal data-taking calibration procedures. The data is stored as part of the ‘environmental’ records. The system has been in regular operation both before and after the shutdown. The design precision of better than $20\mu\text{m}$ has been achieved for most sensors. Figure 6 shows the local x and y position of a laser beam in one of the sensors, plotted as a function of days during the period

following the re-cabling of the MVD. The very large jump in both positions between days 26 and

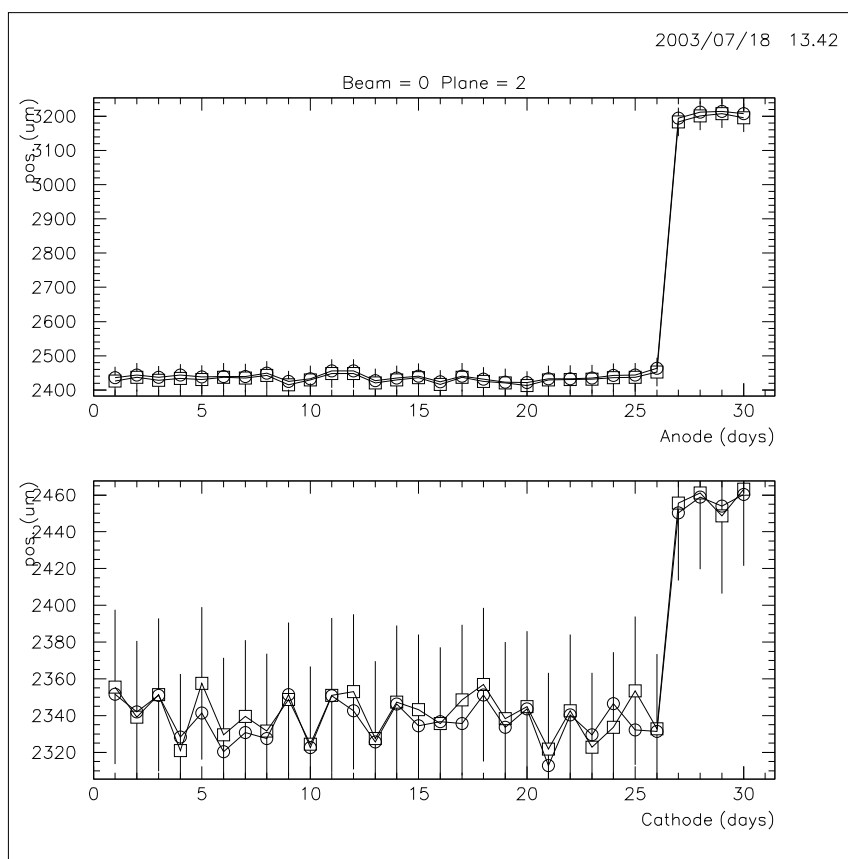


Figure 6: MVD optical alignment system. Position of the laser beam 0 in one sensor, showing a stable position before and after a big ‘jump’.

27 is not a significant movement of the detector but a movement of the laser heads, particularly the angle of tilt with respect to the beam axis. This is correlated with work at the rear end of the MVD and close to the rather delicate mounting of the laser heads. This plot and the full data history taken so far, shows that the MVD structure is very stable, but that the system will probably have to be re-calibrated following a shutdown involving significant work near the rear MVD beam-pipe region.

4.1 Global Track Trigger

The Global Track Trigger is a new trigger component for ZEUS. It combines the information from the existing, transputer based, readout systems for the CTD and STT with that from the new, VME based, readout system of the MVD as early as possible in the ZEUS trigger chain. ZEUS-UK are providing the algorithm development, implementation and evaluation, and have been leading the study of the performance of the GTT system as a whole.

To be compliant with the requirements of the ZEUS DAQ and trigger system the latency for the complete GTT readout and event reconstruction has to be within around 10 ms with reasonably short tails to avoid introducing dead time at the Global First Level Trigger (GFLT).

Previous studies of the GTT latency were made possible by the implementation of a *playback* system, whereby simulated events could be injected into the GTT trigger chain at the VME component interfaces and then sent through the GTT systems and algorithm processes exactly as for real data. Using simulated high transverse energy photoproduction events, with this

run 44535: GTT latency (ms)

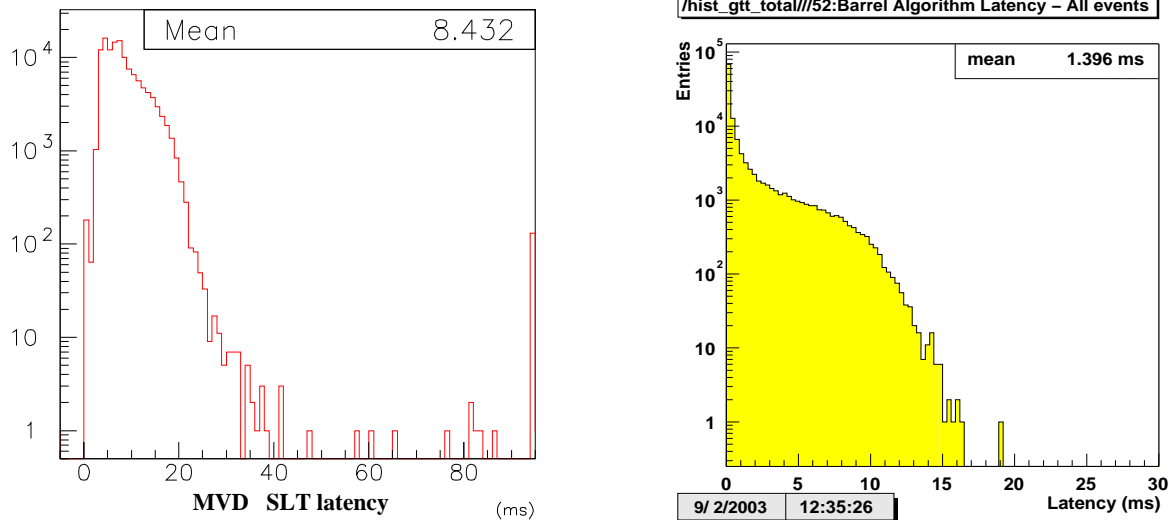


Figure 7: The complete GTT latency at the GSLT including data transfer (left), and the GTT algorithm processing latency (right).

system, the deadtime in the ZEUS trigger chain was seen to be below 2% for an input rate to the ZEUS global first level trigger of 400 Hz.

With the dedicated commissioning luminosity running between October 2002 and February 2003, it was possible to test the performance of the GTT on real ep collision data and tune the data volume cuts and algorithm performance to cope with the higher than expected beam gas background.

The first physics production luminosity run which started in the Autumn of 2003 included tests of GTT operation with real luminosity data under standard data taking conditions. Since, in the commissioning stage, beam related background hits in the MVD were seen to bias the vertex reconstruction, the GTT algorithm is currently running in a mode using only CTD information. Studies are currently underway to modify the algorithm to allow use of MVD hits online.

The performance and stability of the algorithm and GTT system as a whole has been well within the expectation during this period. The complete GTT latency as seen by the ZEUS GSLT for a typical run is shown in Fig.7. The mean latency is 8.4 ms, well within the 10 ms required, with a short tail extending to around 40 ms. The algorithm processing latency for the same run is also shown in Fig.7. The distribution is monotonically falling, since the algorithm runs as a single process, and has a mean of 1.4 ms with a tail extending to around 15 ms for busy events and indicates that the overall GTT latency is dominated by the data transfer times of the large detector data volumes.

The dependence of the mean overall latency on the output rate of the GFLT, typically 50-200 Hz during standard luminosity data taking with the present beam currents shows a strong dependence on the background conditions, but always lies within 10 ms.

Studies using the playback system, which exercises the complete GTT system within the framework of the ZEUS DAQ and trigger system, suggest that the design scenario of operating the GTT with GFLT output rates of up to 500 Hz is achievable.

The GTT event vertex available online is illustrated in Fig.8 and clearly shows events from ep interactions in a vertex peak within ± 25 cm, on the large proton-beam gas background, together with secondary scattering events from the collimator at -80cm. In the newer data since modifications to the collimator during the summer of 2002, the collimator peak is less pronounced.

Using a tight offline selection of DIS events to eliminate the residual beam gas contamination

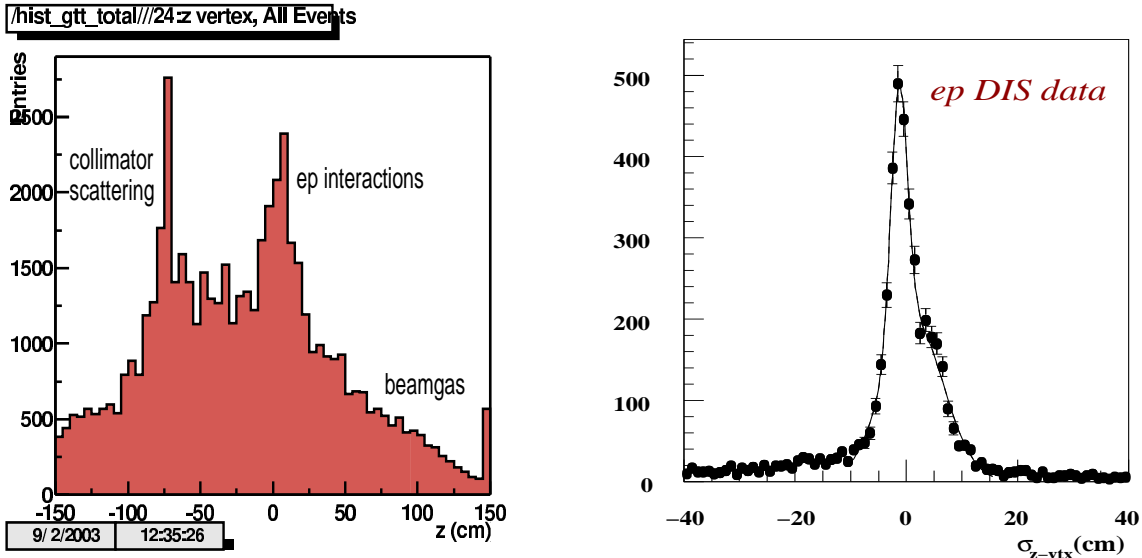


Figure 8: The online CTD-only GTT vertex (left) and the online CTD-only GTT vertex resolution with respect to the offline vertex (right).

of data written offline, the event vertex residual with respect to the offline vertex is also illustrated in Fig.8. The offline vertex has a resolution of around 2 mm. The data have been fitted with a sum of two Gaussians with widths of 1.5cm and 5cm respectively. The 1.5cm distribution is approximately consistent with the 1cm expectation for CTD only vertices in well reconstructed events from Monte Carlo.

The efficiency found using GSLT passthrough events for reconstructing a vertex within ± 25 cm of the offline vertex is found to be 84%.

With the current algorithm, which uses only data from the CTD FADC system, the z information for track and vertex reconstruction is provided only by the stereo layers of the CTD. Due to the large pattern recognition ambiguities that must be quickly resolved, the algorithm is less efficient at reconstructing tracks in events where the charged particle multiplicity is high.

In order to improve the track finding efficiency in these high multiplicity events, the CTD transputer network and readout have been modified by the addition of new transputers to enable the CTD z -by-timing data to be read out into the GTT system. The GTT algorithm has been improved to make use of this data and changes needed to the GTT readout should be completed early in 2004.

5 The HERA Polarimetry Upgrade

One of the objectives of the HERA-II physics programme is the study of the dependence of the neutral and charged current deep inelastic scattering cross sections on the polarisation of the lepton beam. These measurements require excellent precision on the polarisation measurement (better than 1%). For this purpose a polarimetry upgrade project was set up.

At HERA leptons become naturally transversely polarised through the emission of synchrotron radiation (lepton spin flips; Sokolov-Ternov effect). The lepton beam transverse polarisation is converted into longitudinal polarisation near the interaction points by spin rotators. The HERA polarisation is measured by two polarimeters: the TPOL which measures transverse polarisation, located in the HERA-West area close to HERA-B, and the LPOL which measures longitudinal polarisation, located in the HERA-East area close to HERMES. The degree of polarisation is measured by scattering alternately right- and left-circularly polarised laser light off

the polarised lepton beam. The back-scattered Compton photons that are produced are then detected by a calorimeter. The two polarimeters operate differently. Transverse polarisation is determined by measuring the vertical, up-down, asymmetry of the back-scattered photons on the TPOL calorimeter face, while longitudinal polarisation is determined by measuring the energy asymmetry in the LPOL calorimeter.

The TPOL calorimeter is separated horizontally into two halves. The energy sharing between the upper and lower halves is used to determine the impact position of the photon in the vertical direction. The up-down position asymmetry used to determine the polarisation relies on the conversion of the up-down energy asymmetry into a vertical position. This conversion is referred to as the ' $\eta - y$ transformation'. The dominant systematic errors in the polarisation measurement relate either to the linearity of the calorimeter energy response or to the precision with which the $\eta - y$ transformation is known. To determine the transformation precisely, in situ, during data-taking we have implemented a silicon-microstrip detector system. This system is composed of two $60 \times 60 \text{ mm}^2$ silicon-microstrip detectors placed in front of the calorimeter and behind a $1 X_0$ thick lead pre-radiator. The strip pitch of the detector measuring the vertical co-ordinate is $80 \mu\text{m}$. A detector with a strip pitch of $120 \mu\text{m}$ and for which every second strip is read out is used to measure the horizontal coordinate. A high flux of photons enter the TPOL detector. The energy deposited by these photons gives a dose of 5 Mrad per year over an area of only 0.1 mm^2 . In order to identify and correct for the effects of differential radiation damage in the silicon-microstrip detector a scintillating fibre mounted on a precision stage has been installed between the silicon-detector planes and the pre-radiator. The fibre will be scanned periodically across the face of the silicon detector in vertical steps of $2.5 \mu\text{m}$ and will allow differential radiation damage to be identified and corrected for.

The upgraded TPOL detector, having been commissioned using test beams at DESY and at CERN, is now operating routinely. The polarimeter data is integrated into the ZEUS analysis environment and work to provide the high precision measurement of the polarisation has begun. A second iteration of the front-end silicon-detector boards has been built and thoroughly tested at Imperial College, along with some small modifications to the read-out electronics. The improved detector boards will be installed in the TPOL the at the earliest possible opportunity in 2004.

6 Physics analyses

During 2003 sixteen ZEUS physics papers were published or submitted for publication in various journals. In this section, we concentrate on those physics areas where the UK members of ZEUS have been particularly active.

6.1 Inclusive DIS cross-sections and structure function measurements

6.1.1 High Q^2 NC and CC scattering

Deep inelastic scattering (DIS) of leptons off nucleons probes the structure of matter at small distance scales. Two types of DIS interactions are possible at HERA: the neutral current (NC) reactions $e^-p \rightarrow e^-X$ and $e^+p \rightarrow e^+X$, where a photon or Z^0 boson is exchanged and the charged current (CC) interactions $e^-p \rightarrow \nu X$ and $e^+p \rightarrow \bar{\nu}X$, where a W^\pm boson is exchanged. The description of DIS is usually given in terms of three Lorentz invariant quantities: Q^2 , the negative square of the four-momentum transfer, x , the Bjorken scaling variable and y , the fraction of the energy transferred to the proton in its rest frame. These variables are related by $Q^2 = xys$ (neglecting the masses of the incoming particles), where s is the square of the lepton-proton centre-of-mass energy.

The double-differential Born-level cross section for the neutral current deep inelastic scattering processes $e^-p \rightarrow e^-X$ and $e^+p \rightarrow e^+X$, with longitudinally unpolarised beams, is given

by:

$$\frac{d^2\sigma_{\text{Born}}(e^\pm p)}{dx dQ^2} = \frac{2\pi\alpha^2}{xQ^4} [Y_+ F_2(x, Q^2) - y^2 F_L(x, Q^2) \mp Y_- x F_3(x, Q^2)],$$

where $Y_\pm = 1 \pm (1 - y)^2$, α is the QED coupling constant and F_2 , F_L and $x F_3$ are the neutral current structure functions. The NC reduced cross section, $\bar{\sigma}_{NC}$, is defined to be:

$$\bar{\sigma}_{NC}(x, Q^2) = \frac{1}{Y_+} \frac{xQ^4}{2\pi\alpha^2} \frac{d^2\sigma_{\text{Born}}^{NC}}{dx dQ^2}.$$

The double-differential Born-level cross section for the longitudinally unpolarised charged current deep inelastic scattering processes $e^- p \rightarrow \nu X$ and $e^+ p \rightarrow \bar{\nu} X$ are given by:

$$\frac{d^2\sigma_{\text{Born}}^{CC}(e^- p)}{dx dQ^2} = \frac{G_F^2}{2\pi} \frac{M_W^4}{(Q^2 + M_W^2)^2} \times [(u + c) + (1 - y)^2(\bar{d} + \bar{s})],$$

and

$$\frac{d^2\sigma_{\text{Born}}^{CC}(e^+ p)}{dx dQ^2} = \frac{G_F^2}{2\pi} \frac{M_W^4}{(Q^2 + M_W^2)^2} \times [(\bar{u} + \bar{c}) + (1 - y)^2(d + s)],$$

where for example the parton density function (PDF) d is the density of down quarks in the proton at a given x and Q^2 . M_W is the mass of the W boson and G_F is the Fermi constant. The CC reduced cross section, $\bar{\sigma}_{CC}$, is given by:

$$\bar{\sigma}_{CC} = \frac{2\pi}{G_F^2} \left(\frac{Q^2 + M_W^2}{M_W^2} \right)^2 \frac{d^2\sigma_{\text{Born}}^{CC}}{dx dQ^2}.$$

UK physicists have led work on the measurement of the NC and CC high- Q^2 cross sections. The full HERA-I data set has now been analysed and the final papers have been submitted for publication [1, 2]. Figure 9 shows the reduced cross sections for $e^+ p$ and $e^- p$ scattering, as a function of x , for different values of Q^2 . The data are well described by the Standard Model predictions from a ZEUS NLO QCD fit [3]. Figure 10 shows the reduced cross section for $e^+ p$ charged current scattering, again as a function of x , for fixed values of Q^2 . The data are again well described by the Standard Model prediction.

6.1.2 F_L from Radiative Events

UK physicists have also led an analysis of deep inelastic scattering events with hard initial state radiation (ISR) [4]. As the centre-of-mass energy of the subsequent ep interaction is decreased (as opposed to the fixed value for events without initial-state radiation), this allows the possibility of a direct measurement of the longitudinal structure function, F_L . The analysis is technically challenging because of many factors, including the evaluation and subtraction of the background from ep bremsstrahlung events. A subset of the data taken during 1996 has already been used to make measurements of the structure function F_2 which are found to be in good agreement with previous ZEUS results [5]. This agreement was taken as a validation of the ISR method and ISR events have therefore been used to make a direct measurement of F_L . Figure 11 shows the measurement and compares it to the ZEUS NLO QCD fit [3] prediction for F_L and F_2 in this region. QCD predicts that F_L must satisfy $0 < F_L < F_2$ and it is clear from Fig. 11 that this measurement is consistent with the QCD expectation. Further studies are being made prior to publishing this result.

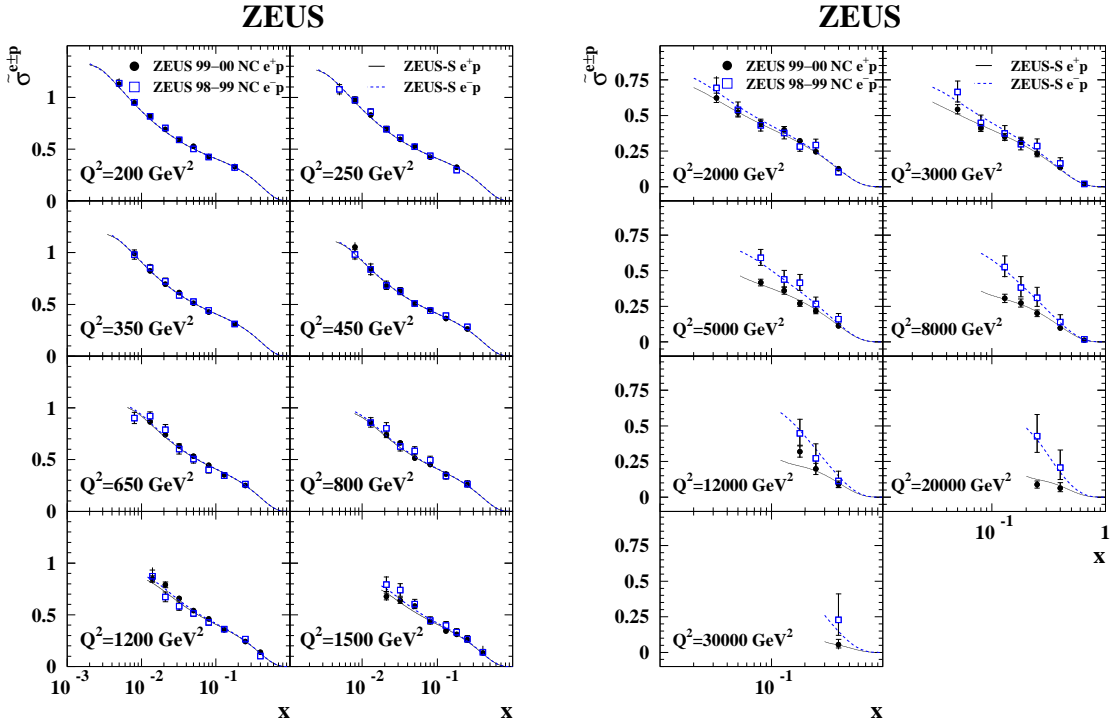


Figure 9: *The reduced cross section for neutral current deep inelastic scattering.*

6.1.3 NLO QCD fits

The UK plays a leading role in the interpretation of the data on the proton structure functions by performing NLO QCD fits, using the DGLAP formalism, to determine the parton density functions and α_S [3]. In the standard (ZEUS-S) fit, the high precision data on neutral current e^+p scattering [6] were fitted together with fixed-target data. A particular focus of this work was the determination of the uncertainties on the parton distributions resulting from experimental sources, particularly from correlated experimental systematic uncertainties from all contributing data sets.

Precise information on PDFs and their uncertainties is necessary in order to make reliable predictions for discovery physics at hadron colliders. The most efficient and compact way of storing information on PDF uncertainties is in terms of eigenvector PDF sets. The errors on the parton distribution parameters are encapsulated in the error matrix (covariance matrix) of the fit. This may be diagonalised and its eigenvalues represent the squared errors on the combinations of parameters which are the eigenvectors. The results of the fit can be summarised as one central PDF set (S) and $2N_{pdf}$ eigenvector PDF sets for the errors, where N_{pdf} is the number of free PDF parameters. For the ZEUS-S fit $N_{pdf} = 11$. These eigenvector PDF sets represent excursions up and down along each of the N_{pdf} eigenvector directions by an amount equal to the error on the corresponding combination of the original PDF parameters, i.e the square-root of corresponding eigenvalue. The eigenvector PDF sets are labelled S_i^+ and S_i^- for each of the $i = 1, N_{pdf}$ eigenvalues. The error on a quantity $F(S)$, which is a function of the PDF parameters, (for example, such a quantity could be a PDF distribution, a structure function or a cross-section) is then calculated from, $\Delta F^2 = \sum_i ((F(S_i^+) - F(S_i^-))/2)^2$, i.e. the value of F is calculated from the parameter sets S_i^+ and S_i^- , exactly as it is for the central set, and then the difference between its value for these two sets gives the error on F due to eigenvector i . These are then simply added in quadrature. The ZEUS-S PDFs, and some model variations on them,

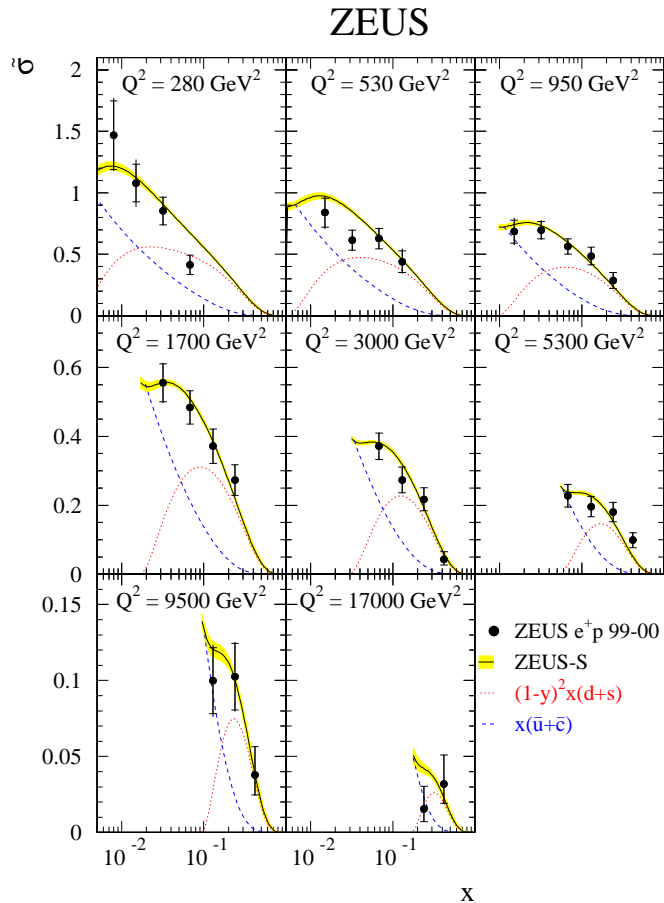


Figure 10: *The reduced cross section for e^+p charged current deep inelastic scattering.*

have now been issued in this form on the Durham database HEPDATA as the ZEUS2002 PDF set (<http://durpdg.dur.ac.uk/hepdata/zeus2002>).

The ZEUS data are crucial for the determination of the gluon and the sea PDFs. In the ZEUS-S fit, the valence PDFs are determined by the fixed target data, which suffer from uncertainties due to the need for heavy target corrections. However, a fit was also made to ZEUS data alone (ZEUS-O fit), with the high Q^2 e^+p data on the CC cross section [7] and the e^-p data on the CC [8] and NC [9] cross sections included to constrain the valence distributions [3]. The precision with which this can be done has been greatly improved by the inclusion of the new e^+p CC [2] and NC [1] data from 99/00. The improvement is particularly good for the less well known high- x d -valence distribution which is directly determined from the high- Q^2 e^+p CC data. Figure 12 compares the valence distributions for the published ZEUS-O fit to those for the ZEUS-O fit including the 99/00 data. The precision of the ZEUS-O fit is limited by statistics rather than systematics, so that further improvement can be expected with higher luminosity HERA-II data.

6.2 Exotic processes

Production of single W bosons at HERA is a rare Standard Model process and an important source of background for searches for physics beyond the Standard Model. The ZEUS and H1 Collaborations have both investigated the processes in which a W boson is produced and decays to an electron or muon and a neutrino. The H1 Collaboration observe an excess of such events

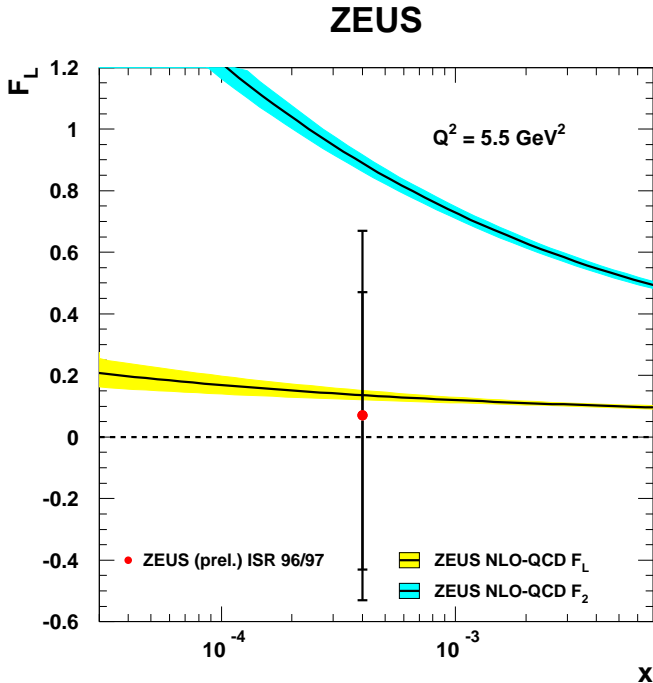


Figure 11: F_L measured using ISR data at $x = 4.0 \times 10^{-4}$.

while the ZEUS measurement is in agreement with the Standard Model prediction. ZEUS-UK physicists have been active in a complementary study of W production at HERA, the case in which the W decays hadronically. A search was made for such events using the full HERA-I data set and a measurement of the cross section was presented in a paper sent to the EPS03 conference.

6.3 Heavy quark production

ZEUS UK groups have been involved in many aspects of the programme to understand heavy quark production, both in data analysis and hardware and software aspects. Analyses investigating the production rate and nature of beauty and charm quarks are making significant contributions in a field which is still poorly understood. The production of charm quarks in DIS and accompanied by jets in photoproduction are now being measured precisely. Details of the ongoing hardware and software projects which will aid in the detection of heavy quarks are discussed in Section 4.

6.3.1 Charm production in DIS

Heavy quarks, particularly charm, are produced copiously in DIS, predominantly via the boson-gluon fusion (BGF) process. This means that measurements of charm production allow, in principle, a direct determination of the gluon density in the proton complementary to extractions of the gluon distribution in QCD fits. Charm is predominantly identified by the decay chain $D^{*+} \rightarrow D^0 \pi^+$, $D^0 \rightarrow K^- \pi^+$ which has low backgrounds but also has small branching ratios. Using a luminosity of 82 pb^{-1} , ZEUS has recently published a measurement of charm production [10] with improved precision and in a kinematic region extending to higher Q^2 than the previous ZEUS results [11].

The data are shown in Fig. 13 as a function of the variable $\eta(D^*)$ and compared with an NLO calculation which gives a good description of the ZEUS data. It should be noted that

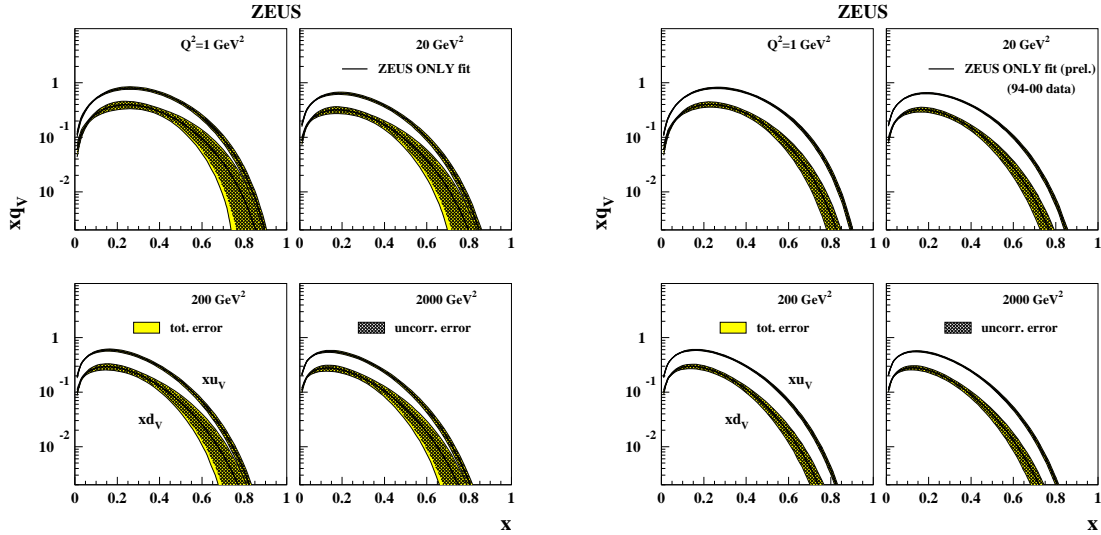


Figure 12: Valence distributions for the published ZEUS-0 fit (left). Valence distributions for the ZEUS-O fit including the 99/00 data (right).

the NLO calculation uses the proton PDF obtained from recent ZEUS NLO QCD fit [3]. This gives a somewhat larger cross section at positive $\eta(D^*)$ and somewhat smaller cross section at negative $\eta(D^*)$ than the CTEQ5F3 PDF [12] used previously. The earlier publications [11] revealed discrepancies in the forward $\eta(D^*)$ direction but this region can now be reasonably well described by a recent fit to the proton PDF as shown in Fig. 13. The data presented here are practically independent of the data used in the ZEUS NLO PDF fit to inclusive DIS data. Further refinement of NLO QCD fits and even the use of these data in future fits may achieve a better description.

By using this data, the charm contribution, $F_2^{c\bar{c}}$, to the proton structure, F_2 can be extracted. Owing to experimental limitations, the D^* meson is restricted to the central region of the detector with transverse momentum larger than 1.5 GeV. Cross sections are measured differentially in Q^2 and x and compared with NLO QCD. The NLO QCD is then used to extract $F_2^{c\bar{c}}$:

$$F_{2,\text{meas}}^{c\bar{c}} = \frac{\sigma(x, Q^2)_{\text{meas}}}{\sigma(x, Q^2)_{\text{theo}}} F_{2,\text{theo}}^{c\bar{c}} \quad (1)$$

The extrapolation factors to the full D^* phase space vary between 4.7 at low Q^2 and 1.5 at high Q^2 . The extracted $F_2^{c\bar{c}}$ values are shown compared with an NLO QCD prediction in Fig. 14.

The data show a step rise to low x indicative of a large gluon density in the proton. The data are well described by the NLO prediction demonstrating the consistency of the gluon density extracted in PDF fits and “measured” more directly here. At low Q^2 , the data, specifically the double differential cross sections, $\sigma(x, Q^2)_{\text{meas}}$, measured within the acceptance of the detector, have reached sufficient precision such that they can be used further to constrain the gluon density in the proton.

Use of other decay channels along with very high-statistics measurements of heavy quark production in DIS will be major goals with new data from the upgraded HERA accelerator and ZEUS experiment. UK physicists are taking a leading role in both activities.

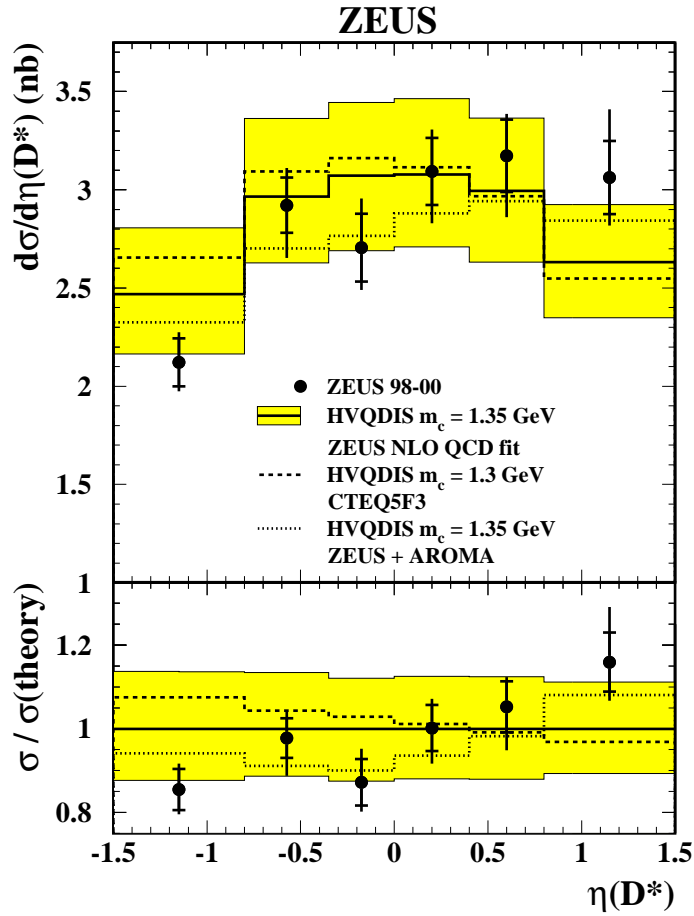


Figure 13: Differential D^* cross section as a function of $\eta(D^*)$ compared to an NLO QCD calculation. Predictions from the ZEUS NLO QCD fit are shown for $m_c = 1.35$ GeV (solid line) with its associated uncertainty (shaded band). Predictions using the CTEQ5F3 PDF (dashed-dotted line) and an alternative hadronisation scheme (dotted line) are displayed. The ratios of the cross sections to the central NLO prediction are also shown beneath the plot.

6.3.2 Charm production with jets

With the larger statistical sample in the photoproduction regime ($Q^2 < 1 \text{ GeV}^2$), charm production accompanied by jets is providing a detailed picture of many aspects of QCD and, in particular, the charm content of the photon. The first measurement of charm quarks inside jets was published in 1999 [13], with UK physicists as principal authors. The results showed for the first time that charm is produced copiously in resolved-photon events. Building on these results, resolved-photon processes have been studied further in order to understand whether the charm quark is an active parton in the photon or is produced only in the hard scatter.

A recent measurement [14] of the dijet scattering angle, θ^* , in D^* production is shown in Fig. 15. The distribution is sensitive to the propagator in the hard scatter and thereby sensitive to the nature of the sub-process. The tagged D^* meson is associated with one of the jets and the scattering angle of this jet is defined with respect to the proton direction. The angular distribution, enriched in direct photon processes ($x_\gamma^{\text{obs}} > 0.75$), exhibits a symmetric distribution with a shallow rise to high values of $\cos \theta^*$. This is indicative of the exchange of a quark in the hard sub-process with the charm produced via the boson-gluon fusion process. At low x_γ^{obs} , where the sample is enriched in resolved photon processes, the data are asymmetric, exhibiting

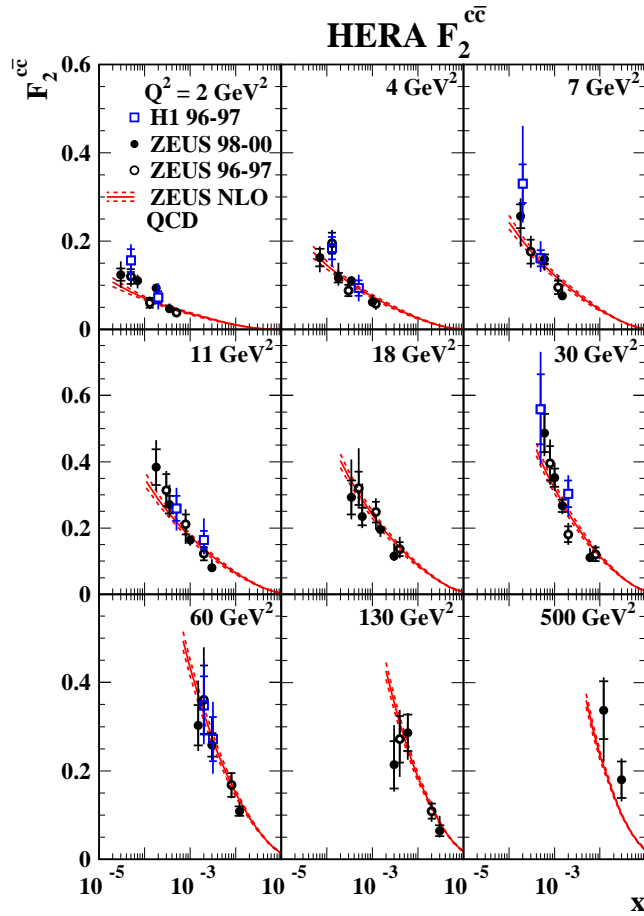


Figure 14: The measured $F_2^{c\bar{c}}$ at Q^2 values between 2 and 500 GeV^2 as a function of x . The current data (solid points) are compared with the previous H1 (triangles) and ZEUS (open points) measurements.

a rapid rise to negative $\cos\theta^*$. This demonstrates that the charm comes from the photon and exchanges a gluon in the hard process. The prediction of NLO in which charm is produced in the hard sub-process and is not an active flavour in the structure function, lies below the data. The description of the data could be improved by including a charm component in a NLO fit of the photon PDF.

The presence of heavy quarks in the evolution of the photon structure offers a promising window for understanding the development of QCD structure, splitting functions and threshold effects. The ability at HERA to select concurrently on jet transverse energy, E_T^{jet} , photon virtuality and x_γ^{obs} , as well as to compare heavy flavour jets with untagged jets, makes it uniquely suitable for detailed studies in this area. Thus heavy flavour jet production will be a growth area, and is a major driving force behind the UK's involvement in the MVD. The GTT will play a vital part in allowing these events to be saved at relatively low E_T^{jet} even after the upgrade, particularly if charm enrichment can be implemented.

6.4 QCD and the hadronic final state

The UK group continues to play a significant role in the study of QCD and the hadronic final state at ZEUS. New analyses are beginning on the prompt photon production in photoproduction using the complete HERA I data sample and work on strange particle production, in particular

ZEUS

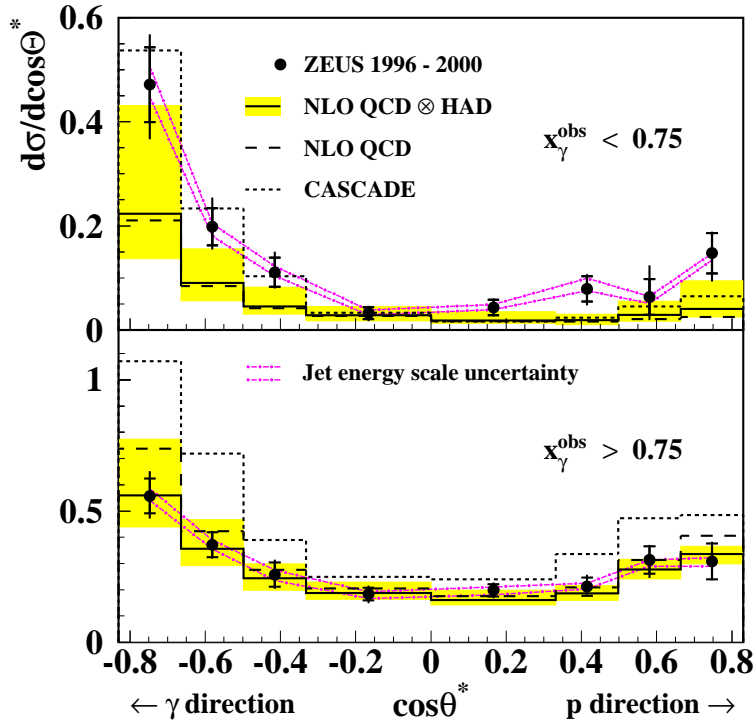


Figure 15: Measurement of the dijet angular distributions in charm photoproduction at HERA.

K_s and Λ production mechanisms in high E_T photoproduction, reported last year continues. In addition UK personnel are leading a new cross group initiative to make use of the current ZEUS data on jet production in DIS and photoproduction in the ZEUS fit of the proton parton distribution functions.

6.5 Event shapes in DIS

The recent revival of interest in the study of event shape measurements prompted by theoretical developments in the understanding of hadronisation or power corrections. Power corrections allow perturbative QCD (pQCD) calculations to be extended into the region of low momentum transfers using approximations to higher-order graphs. At HERA, the Q^2 scale can be varied over four orders of magnitude enabling power corrections (proportional to $1/Q^n$) to be studied in detail. ZEUS results from the UK group, published last year [15], compared the data for the mean value of many event shape variables, such as the thrust and jet broadening variables, with theoretical expectations for the power corrections and the effective coupling $\alpha_0(\mu_I)$, specified at the infra-red matching scale $\mu_I = 2$ GeV, and $\alpha_s(M_Z)$ was extracted.

This demonstrated that theoretical uncertainties due to uncalculated higher-order x -dependent terms appear to be significant, especially for the jet broadening. To generate further insight into both perturbative and non-perturbative QCD mechanisms in the generation of hadronic final states at high energies the published results are being extended to include comparisons of the event shape distributions themselves with more recent resummed calculations [16] and it is hoped that results will be ready early in the new year.

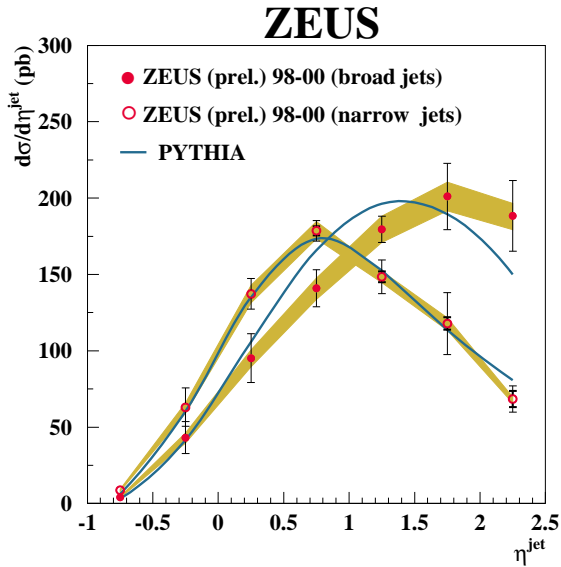


Figure 16: The dependence of the cross section versus η for inclusive jet production for “broad” and “narrow” jets.

6.6 The substructure dependence of jet cross sections

Previous results [17] on inclusive jet and dijet production in photoproduction concentrated on the detailed study of the jet production kinematics in order to probe the QCD hard sub process and study the hadronic structure of the photon.

New results using the full 1998-2000 data sample additionally make use of the internal structure of the jets themselves to try to further constrain the event kinematics and study the properties of the QCD sub process.

The substructure of the jets is measured using the integrated jet shape, ψ , defined as the fraction the jet transverse energy, E_T , in a cone in $\eta - \phi$ space of radius r ,

$$\psi(r) \equiv E_T(r)/E_T^{\text{jet}},$$

and also the subjet multiplicity, defined as the number of subjets found when running the k_\perp jet algorithm over the objects assigned to the jet with different values of the jet resolution parameter, y_{cut} . As the radius r is increased, so a larger fraction of the jet E_T is included in the integrated jet shape, and as the resolution parameter y_{cut} is reduced, so more objects are resolved within the jet.

Since jets initiated where the primary parton is a gluon tend to be broader than jets where the primary parton is a quark, placing a cut on either the integrated jet shape or the subjet multiplicity enables the separation of the jets into samples enhanced respectively in gluons (“broad” jets) or quarks (“narrow” jets).

Figure 16 shows the cross section for the inclusive production of broad and narrow jets as a function of the pseudo rapidity of the jet, η^{jet} , compared to the predictions from the PYTHIA Monte Carlo generator [18] and illustrate that gluon jets tend to be produced more in the forward region of the detector.

For events where two jets are detected, the sample can be further divided into events with either two broad jets, two narrow jets, or one broad and one narrow jet.

Figure 17 shows distributions of $\cos \theta^*$, where θ^* is the angle of the dijet axis with respect to the beam direction in the dijet centre of mass frame. Figure 17 (left) shows the modulus of $\cos \theta^*$ for the broad-broad and narrow-narrow configurations clearly illustrating that the broad-broad configuration dominated by gluon-exchange processes rises more steeply, as expected for a spin 1 propagator, whereas the narrow-narrow configuration has the more shallow rise of the spin 1/2 propagator.

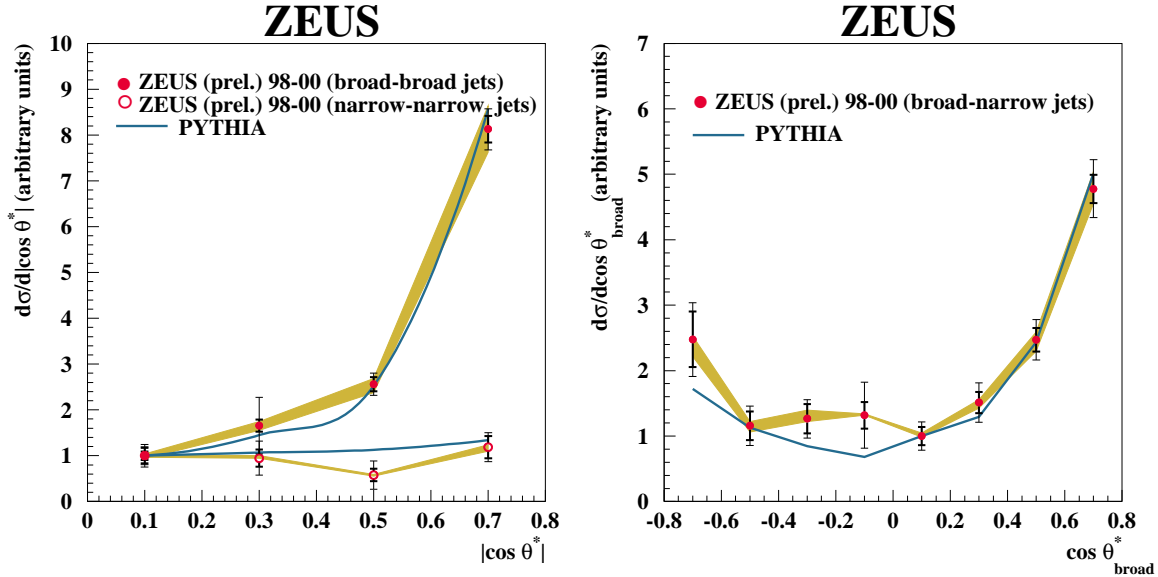


Figure 17: The dependence of the cross section versus $\cos \theta^*$ for dijet jet production for various configurations of “broad” and “narrow” jets.

Since the broad-narrow configuration enables the gluon jet to be distinguished from the quark jet the signed value of $\cos \theta^*$ can be measured where θ^* is measured with respect to the broad jet. Figure 17 (right) shows the $\cos \theta^*$ distribution for these broad-narrow events. The distribution clearly rises more rapidly in the forward direction, $\cos \theta^* \rightarrow 1$, consistent with the dominant resolved process being $qg \rightarrow qg$ where the incoming gluon is from the proton.

6.6.1 Virtual-photon structure

It has been long established that the real photon, $Q^2 = 0$, has a partonic structure, while at high Q^2 it is commonly considered to be a point-like particle and used as a probe of the partonic structure of hadronic targets. Even though considerable progress from the theoretical and experimental sides has recently been made in investigating the structure of virtual photons, the PDFs of the virtual photon are less well known than those of the real photon.

The differential dijet cross section, $d\sigma/dQ^2$, for $E_T^{\text{jet},1} > 7.5$ GeV, $E_T^{\text{jet},2} > 6.5$ GeV, $-3 < \eta^{\text{jet}} < 0$ and $0.2 < y < 0.55$ in the range $0.1 < Q^2 < 2000 \text{ GeV}^2$ and in the photoproduction region $Q^2 < 1 \text{ GeV}^2$ for the direct-enhanced region ($x_\gamma^{\text{obs}} > 0.75$) and the resolved-enhanced region ($x_\gamma^{\text{obs}} < 0.75$), together with the total dijet cross section have been measured. The measurements are precise and cover a wide range of photon virtualities, including the transition region from photoproduction to DIS. The measured cross sections fall by more than four orders of magnitude over this Q^2 range. The cross section for $x_\gamma^{\text{obs}} < 0.75$ falls more rapidly than that for $x_\gamma^{\text{obs}} > 0.75$. Even though the total cross section is dominated by interactions with ($x_\gamma^{\text{obs}} > 0.75$) for $Q^2 \geq 10 \text{ GeV}^2$, there is still a contribution of about 24% from low- x_γ^{obs} events even for Q^2 as high as 500 GeV^2 .

The Q^2 dependence of the direct- and resolved-enhanced components of the dijet cross section has been studied in more detail using the ratio

$$R = \frac{d\sigma}{dQ^2(x_\gamma^{\text{obs}} < 0.75)} / \frac{d\sigma}{dQ^2(x_\gamma^{\text{obs}} > 0.75)}.$$

The experimental and theoretical uncertainties largely cancel in the ratio, so that a more stringent test of the theory is possible. Figure 18 shows the ratio R as a function of Q^2 in three different

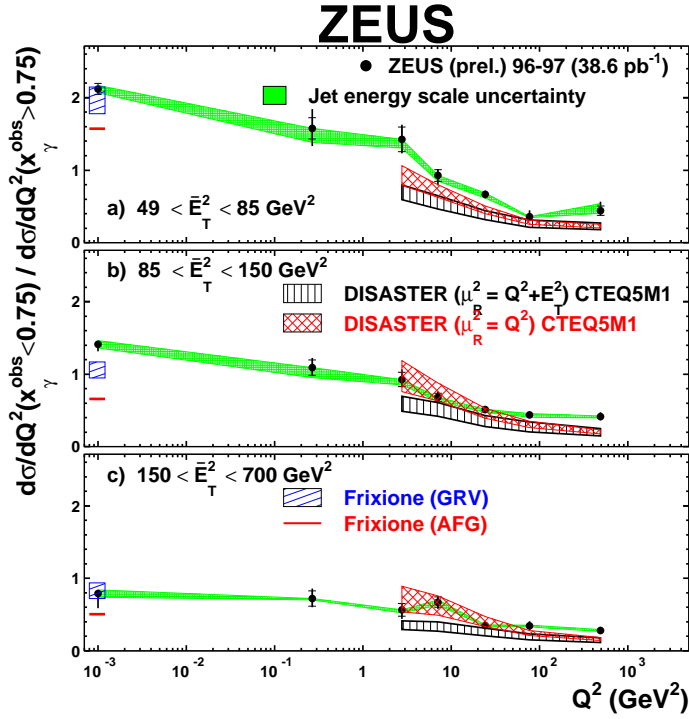


Figure 18: Measured ratio R as a function of Q^2 in different regions of E_T^2 (black dots). The NLO QCD calculations of DISASTER [19], DISASTER++ [20] and that of Frixione *et al.* are also shown.

regions of $\overline{E_T^2}$. The Q^2 dependence of the data is stronger at low $\overline{E_T^2}$, where the photon is expected to have structure, than for higher $\overline{E_T^2}$, showing that the resolved contribution is indeed suppressed at low Q^2 as $\overline{E_T^2}$ increases.

The NLO predictions fail to describe the Q^2 dependence of R : the calculations significantly underestimate the measured ratio for $Q^2 < \overline{E_T^2}$. This disagreement between the data and the NLO calculations decreases as $\overline{E_T^2}$ increases, but, at the highest Q^2 and $\overline{E_T^2}$ the theory still falls below the data.

6.6.2 Rapidity Gap between Jets in Photoproduction

Events produced in hadronic collisions with two jets of high transverse energy separated by a large rapidity gap containing little or no energy provide an ideal environment to study the mechanism of colour-singlet exchange in a regime where perturbative QCD should be applicable. The dominant production mechanism for such events is a hard interaction between partons from the incoming hadrons interacting via a quark or gluon propagator. This exchange of colour quantum numbers gives final state jets that are colour connected both to each other and to the hadronic remnants. This leads to energy flow that populates the pseudorapidity region both between the hadronic remnants and between the jets themselves. Events with a large rapidity gap between the jets would then be a signature for the exchange of a colour singlet. This exchanged object could be either an electroweak boson, or some strongly-interacting Pomeron-like object. The high transverse energy provides a perturbative hard scale at each end of the colour-singlet exchange, so that the cross section should be fully calculable in perturbative QCD.

In addition, a class of recently discovered logarithms [21] which affect event observables such as energy flow are expected to play a significant rôle in predictions for events with a large

rapidity gap. So called *global* logarithms arise due to soft gluon radiation directly into the gap, whereas *non-global* logarithms arise from secondary emission of soft gluons into the gap where the primary emission is not necessarily into the gap. Calculations for this data have recently become available [22].

The gap fraction – the fraction of events with a rapidity gap containing less than some threshold in transverse energy – falls for increasing rapidity gap, but levels out as the size of the gap increases. The predictions of leading log Monte Carlos, PYTHIA and HERWIG without colour-singlet exchange show an approximately exponential dependence on the size of the rapidity gap, consistent with the purely statistical behaviour seen in studies of rapidity gaps in e^+e^- annihilation. The predictions lie below the data for larger rapidity gap values. The inclusion of an explicit QCD colour-singlet-exchange contribution, improves the comparison with the present data, although the model still lies below the data for larger rapidity gaps.

Figure 19 shows the gap fraction as a function of $\Delta\eta$ compared to the calculation of Appleby and Seymour for four values of the threshold for the allowed transverse energy in the gap.

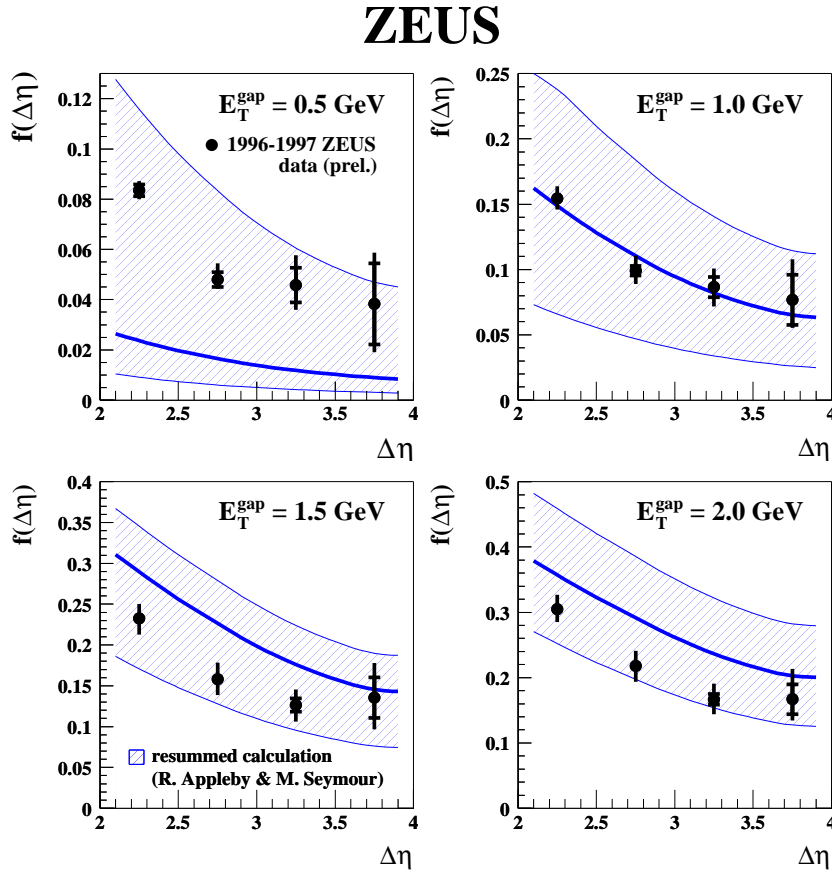


Figure 19: The gap fraction, f , as a function of $\Delta\eta$ compared to the resummed calculation of Appleby and Seymour. The data are shown as the solid points, where the inner error bar shows the statistical uncertainty and the outer error bar shows the statistical and systematic uncertainty added in quadrature.

Although the general shape of the data is reproduced, the trend as a function of the transverse energy threshold, E_T^{gap} , is steeper in the calculation than in the data. In particular, the calculation appears significantly below the data for small E_T^{gap} , where the theoretical uncertainties arising from the renormalisation scale dependence are largest and above the data for larger E_T^{gap} .

Progress on the analysis is continuing and a paper is expected to be ready for publication early in the new year.

6.6.3 Multijet production in photoproduction

The study of multijet production provides sensitive tests of pQCD at intrinsically higher order in the strong coupling constant. In resolved events, it is possible for further hard scatters to take place between the proton and photon remnants. This is known as multiple parton scattering, or multi-parton interactions.

The photoproduction of events with both three or four jets in the final state continues to be studied. Results [23] suggest a large contribution from low- x_γ partons, which tend to be boosted further forward compared to those at high x_γ (for the same fraction of the proton momentum, x_p , entering the hard scatter). Monte Carlo predictions with no simulation of the underlying event are unable to describe the distribution of the data.

Inclusion of multi-parton interaction models lead to a significantly improved description of the data. Progress continues to be made in understanding the interplay of the models of underlying events with the hard sub process and results are expected to be ready for publication in the new year.

6.7 Prompt photons in deep inelastic scattering

A first study of prompt photon production, with and without an accompanying jet, in deep inelastic scattering is nearing completion. The cross sections have been compared with some new NLO QCD calculations by Kramer and Spiesberger.

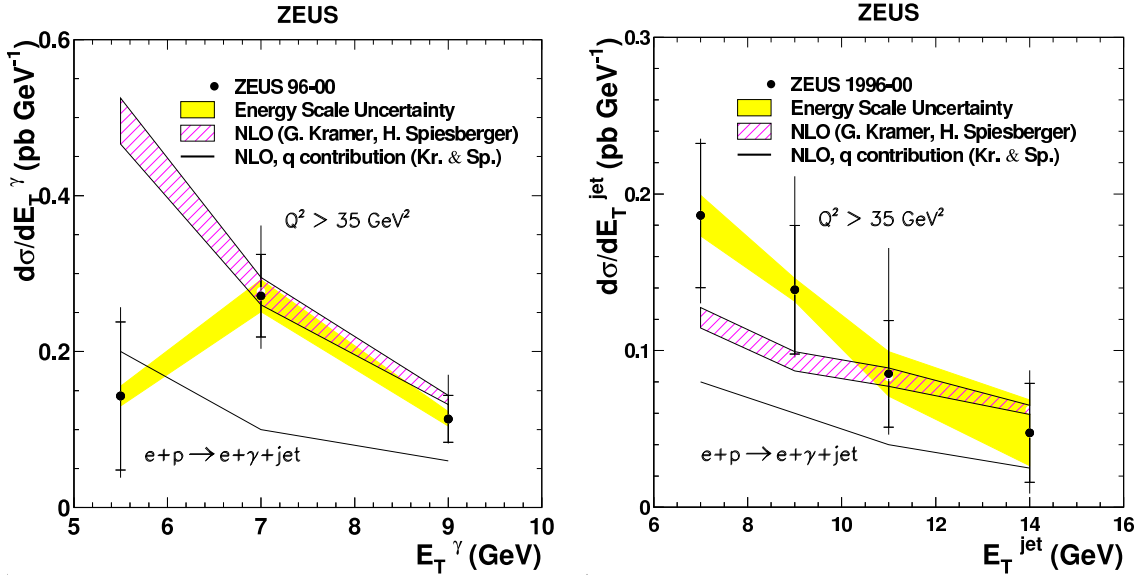


Figure 20: Prompt photon production in DIS $e + p \rightarrow e + \gamma + jet + X$. LH plot E_T^γ spectrum; RH plot E_T^{jet} spectrum.

Figure 20 shows the cross section versus E_T for both the prompt photon and the jet in events where both the photon and jets are observed compared to the NLO calculation. The predicted parton level cross section is somewhat above the data, although the calculation does not include any contribution from hadronisation effects, which estimates indicate could reduce the cross section by 30 to 40%. Also shown is the contribution to the calculation where the photon is radiated from the scattered quark from the proton, the remaining contribution coming

from photons radiated from the lepton. Interference effects between these two contributions contribute approximately 2% of the total.

Further insight into these processes will clearly benefit from the higher integrated luminosities expected at HERA II.

References

- [1] ZEUS Collaboration, S. Chekanov et al., *High- Q^2 neutral current cross sections in e^+p deep inelastic scattering at $\sqrt{s} = 318 \text{ GeV}^2$* , DESY-03-214, to be submitted to Phys. Rev. D.
- [2] ZEUS Collaboration, S. Chekanov et al., *Measurements of high- Q^2 charged current cross-sections in e^+p deep inelastic scattering at HERA*, DESY-03-093, accepted by Eur.Phys.J
- [3] ZEUS Collaboration, S. Chekanov et al., *A ZEUS next-to-leading-order QCD analysis of data on deep inelastic scattering*, Phys. Rev. D. **67** (2003) 012007.
- [4] ZEUS Collaboration, S. Chekanov et al., *Measurement of the proton structure functions F_2 and F_L using initial state radiative events at HERA*, Abstract 502, Submitted to Int. Europhysics Conf. on High Energy Physics, July 2003, Aachen.
- [5] ZEUS Collaboration, S. Chekanov et al., *Measurement of the proton structure function F_2 using initial-state radiative events at HERA*, Abstract 771, Submitted to XXXIst Int. Conf. on High Energy Physics, July 2002, Amsterdam.
- [6] ZEUS Collaboration, S.Chekanov et al., *Measurement of the neutral current cross-section and F_2 structure function for deep inelastic e^+p scattering at HERA* Eur. Phys. J. **C21** (2001) 443.
- [7] ZEUS Collaboration, J.Breitweg et al., *Measurement of High Q^2 Charged-Current e^+p Deep Inelastic Scattering Cross Sections at HERA*, Eur. Phys. J. **C12** (2000) 411.
- [8] ZEUS Collaboration, S. Chekanov et al., *Measurement of High- Q^2 Charged Current Cross Sections in e^-p Deep Inelastic Scattering at HERA*, Phys.Lett. **B539** (2002) 197-217; Erratum: Phys.Lett. **B552** (2003) 308.
- [9] ZEUS Collaboration, S. Chekanov et al., *Measurement of High- Q^2 Neutral Current Cross Sections in e^-p Deep Inelastic Scattering at HERA*, Eur. Phys. J. **C28** (2003) 175.
- [10] ZEUS Collaboration, J. Breitweg et al., *Measurement of $D^{*\pm}$ production in deep inelastic $e^\pm p$ scattering at HERA*, DESY-03-115, accepted by Phys. Rev. D.
- [11] ZEUS Collaboration, J. Breitweg et al., *Measurement of $D^{*\pm}$ production and the charm contribution to F_2 in deep inelastic scattering at HERA*, Euro. Phys. J. **C 12** (2000) 35.
- [12] CTEQ Collaboration, H.L.Lai et al., Euro. Phys. J. **C 12** (2000) 375.
- [13] ZEUS Collaboration, J. Breitweg et al., *Measurement of inclusive $D^{*\pm}$ and associated dijets cross sections in photoproduction at HERA*, Euro. Phys. J. **C 6** (1999) 67.
- [14] ZEUS Collaboration, S.Chekanov et al., *Dijet angular distributions in photoproduction of charm at HERA*, Phys. Lett. **B565** (2003) 87.
- [15] ZEUS Collaboration, S.Chekanov et al., *Measurement of event shapes in deep inelastic scattering at HERA*, DESY-02-198, to be published.
- [16] M. Dasgupta and G.P. Salam, JHEP 0208 (2002) 32.
- [17] ZEUS Collaboration, S.Chekanov et al., *Dijet photoproduction at HERA and the structure of the photon*, Eur. Phys. J. **C23** (2002) 4, 615-631,
ZEUS Collaboration; S. Chekanov et al., *Scaling violations and determination of α_s from jet production in $\gamma - p$ interactions at HERA*, Phys. Lett. **B560** (May 2003) 7-23.

- [18] T. Sjöstrand, *Comp. Phys. Comm.* **82** (1994) 74.
- [19] M.H. Seymour, *DISENT Program Manual, Version 0.1* (1997).
- [20] D. Graudenz, *DISASTER++ Program Manual, Version 1.0.1* (1997).
- [21] R.B.Appleby and G.P.Salam, *Theory and phenomenology of non-global logarithms*, hep-ph/0305323.
- [22] R.B. Appleby and M.H. Seymour, *JHEP* 0309 (2003) 56.
- [23] C.Gwenlan, *Multi-jet production in $\gamma - p$* , proceedings of DIS02, Cracow (2002).

Appendices

UK Ph D Theses submitted in 2003

1. S Robins (Bristol), *Charm production in deep inelastic scattering at HERA* (March 2003).
2. M S Bell (Glasgow), *Prompt photon production in deep inelastic scattering at HERA* (May 2003).
3. J R Goncalo (Imperial), *Measurement of the high- Q^2 neutral current deep inelastic scattering cross sections with the ZEUS detector at HERA*. (October 2003)
4. C Gwenlan (UCL), *Jets and Energy Flow in Photoproduction using the ZEUS Detector at HERA* (September 2003).

Talks on ZEUS and ZEUS-related physics at major conferences

1. J Cole (Bristol), *F₂/FL from ISR data*, DIS03 conference, St. Petersburg, Russia, April 2003.
2. M Wing (Bristol), *Heavy flavour production with leptons and hadrons*, XXIII Physics in Collision conference, DESY, Zeuthen, Germany, June 2003.
3. M Wing (Bristol), *Recent results and progress from ZEUS*, Presentation to Physics Research Council, DESY, Hamburg, October 2003.
4. M Wing (Bristol), *Charm production at ZEUS*, Workshop on heavy quark physics at the upgraded HERA collider, Weizmann Institute, Israel, October 2003.
5. P J Bussey (Glasgow), *Jet production and α_s measurements at HERA*, Photon 03 conference, Frascati, Italy, April 2003.
6. P J Bussey (Glasgow), *Virtual photon structure at HERA*, Photon 03 conference, Frascati, Italy, April 2003.
7. D H Saxon (Glasgow), *Prompt photon production with associated jets at HERA*, EPS meeting, Aachen, July 2003.
8. A Tapper (Imperial), *Constraining particle density functions using HERA data*, DESY Forum on F_2 and QCD fits at HERA, DESY, Hamburg, Germany, March 2003.
9. A Tapper (Imperial), *Probing proton structure in high-energy ep collisions*, New Trends in High-Energy Physics, Crimea, Ukraine, May 2003.
10. A Cooper-Sarkar (Oxford), *The Structure of the Proton*, Invited talk to the Royal Society of Edinburgh, February 2003.
11. A Cooper-Sarkar (Oxford), *Results on Structure Function Measurements and QCD fits*, Low- x Meeting, Naphlion, Greece, June 2003.
12. R Devenish (Oxford), *Experimental aspects of structure functions, low- x and hard diffraction*, summary talk for DIS03 Working Group A, St Petersburg, April 2003.
13. J Ferrando (Oxford), *Searches for single top production in ep collisions*, International Europhysics Conference on HEP, Aachen July 2003.
14. C Gwenlan (Oxford), *Review of Jet Results from HERA*, International Symposium on Multiparticle Dynamics, Cracow, Sept. 2003.
15. M Sutton (Oxford), *Rapidity gaps and energy flows between jets*, talk at DIS03, St Petersburg, April 2003.

16. M Sutton (Oxford), *Scaling violations in inclusive jet production at HERA and measurement of α_s* , talk at DIS03, St Petersburg, April 2003.
17. M Sutton (Oxford), *The ZEUS Global Tracking Trigger barrel algorithm and performance*, talk at the IEEE Realtime 2003 conference, Montreal, May 2003.
18. M Sutton (Oxford), *Jets*, Low- x Meeting, Naphthlion, Greece, June 2003.
19. J M Butterworth (UCL), *Studying QCD in the final state of high energy collisions*, hep-ex/0309063, Summary of the Final States Sessions of the XI International Workshop on Deep Inelastic Scattering, St. Petersburg, April 2003.

ZEUS Collaboration publications in 2003

1. *Search for single-top production in ep collisions at HERA*, DESY-03-012 (January 2003), Physics Letters B 559 (May 2003) 153 - 170.
2. *Addendum: Search for single-top production in ep collisions at HERA*, (DESY-03-012) DESY-03-188 (November 2003), to be submitted to Physics Letters B.
3. *Dijet angular distributions in photoproduction of charm at HERA*, DESY-03-015 (January 2003), Physics Letters B 565 (2003) 87-101.
4. *A search for resonance decays to lepton+jet at HERA and limits on leptoquarks*, DESY-03-041 (March 2003), Physical Review D 68 (2003) 052004.
5. *Jet production in charged current deep inelastic e^+p scattering at HERA*, DESY-03-055 (June 2003), European Phys. Journal C 31 (2003) 149-164.
6. *Measurement of deeply virtual Compton scattering at HERA*, DESY-03-059 (April 2003), Physics Letters B 573 (2003) 46-62.
7. *Measurement of high- Q^2 charged current cross sections in e^+p deep inelastic scattering at HERA*, DESY-03-093 (July 2003), accepted by European Phys. Journal C.
8. *Measurement of the open-charm contribution to the diffractive proton structure function*, DESY-03-094 (July 2003), Nuclear Physics B 672 (2003) 3-35.
9. *Observation of $K_s^0 K_s^0$ resonances in deep inelastic scattering at HERA*, DESY-03-098 (July 2003), Physics Letters B 578 (2004) 33-44.
10. *Measurement of $D^{*\pm}$ production in deep inelastic $e^\pm p$ scattering at HERA*, DESY-03-115 (August 2003), accepted by Physical Review D.
11. *Bose-Einstein correlations in one and two dimensions in deep inelastic scattering*, DESY-03-176 (October 2003), accepted by Physics Letters B.
12. *Isolated τ leptons in events with large missing transverse momentum at HERA*, DESY-03-182 (October 2003), accepted by Physics Letters B.
13. *Search for QCD-instanton induced events in deep inelastic ep scattering at HERA*, DESY-03-201 (December 2003), submitted to European Physical Journal C.
14. *Beauty photoproduction measured using decays into muons in dijet events in ep collisions at $\sqrt{s} = 318$ GeV*, DESY-03-212 (December 2003), submitted to Physical Review D.
15. *High- Q^2 neutral current cross section in e^+p deep inelastic scattering at $\sqrt{s} = 318$ GeV*, DESY-03-214 (December, 2003), submitted to Physical Review D.
16. *Search for contact interaction, large extra dimensions and finite quark radius in ep collisions at HERA*, DESY-03-218 (December 2003), submitted to Physics Letters B.
17. *Photoproduction of $D^{*\pm}$ mesons associated with a leading neutron*, DESY-03-221 (December 2003).

Papers by ZEUS-UK authors on ZEUS-related topics

1. P J Bussey (for the ZEUS and H1 Collaborations), *Jet physics at HERA*, Nucl. Phys. **A721** 821c-824c (2003)
2. P J Bussey (for the ZEUS and H1 Collaborations), *Heavy flavour physics at HERA*, Nucl. Phys. **A721** 825c-828c (2003)
3. K Long & K P Schuler, *Polarisation measurements on e^\pm beams*, Nuclear Instruments and Methods in Physics Research **A494** 75-80 (2002).
4. A Cooper-Sarkar & R Devenish, *The rise and fall of F_2 at low- x* , Acta Physica Polonica **B34** 2911 (2003). Invited contribution to the Festschrift for Jan Kwiecinski.